Chemical and Process Engineering 2021, 42 (3), 209–222
DOI: 10.24425/cpe.2021.138926

The homogeneity of immiscible liquid–liquid dispersion in a vessel agitated by Rushton turbine

Roman Formánek*, Radek Šulc

Czech Technical University in Prague, Faculty of Mechanical Engineering,
Department of Process Engineering, Technická 4, 160 00 Prague, Czech Republic

The homogeneity of an immiscible liquid–liquid system was investigated in a baffled vessel agitated by a Rushton turbine. The dispersion homogeneity was analyzed by comparing Sauter mean diameters and drop size distribution (DSD) determined in different measured regions for various impeller speeds. The sizes of droplets were obtained by the in-situ measurement technique and by the Image Analysis (IA) method. Dispersion kinetics was successfully fitted with Hong and Lee (1983) model. The effect of intermittency turbulence on drop size reported by Bałdyga and Podgórska (1998) was analyzed and the multifractal exponent α_{FT} was evaluated.

Keywords: liquid–liquid dispersion homogeneity, Sauter mean diameter, drop size distribution, Rushton turbine, intermittency turbulence

1. INTRODUCTION

The agitation of immiscible liquids or solid suspensions is a frequent operation in chemical and metallurgical industries. The product quality yield and economy of the processes are significantly affected by mixing conditions. Prediction of mean drop size distribution (DSD) during agitation is fundamental for processes in many branches of industry where mass transfer is crucial.

The experimental drop size measurement has been still challenging. The experimental techniques can be divided into two main groups: 1) indirect ex-situ measurement of dispersion sample withdrawn from a dispersion device, and 2) in-situ measurement allowing direct measurement at the operating conditions utilizing invasive or non-invasive optical observation – e.g. high-speed imaging (Maaß and Kraume, 2012), in situ video probe with image analysis (Khalil et al., 2010), endoscope measurement technique (Kraume et al., 2004), interferometric particle imaging and shadowgraph method (Jasikova et al, 2018). The tomography techniques based on electrical impedance (e.g. Malík et al., 2019) or electrical resistance (e.g. Maluta et al., 2020) are used for the measurement of radial and axial profiles of the light immiscible liquid volumetric fraction.

The size of drops formed in the immiscible liquid–liquid (l–l) system in a mechanically agitated vessel depends on many factors such as vessel configuration and impeller type. The effect of these factors was

* Corresponding author, e-mail: Roman.Formanek@fs.cvut.cz

investigated and reported by many authors (e.g. Kraume et al, 2004; Pacek et al., 1999; Zhou and Kresta, 1998). The dispersed liquid–liquid systems are usually characterized by Sauter mean diameter and drop size distribution. Based on Hinze –Kolmogorov theory (Kolmogorov, 1949; Hinze, 1955), the relation between equilibrium Sauter mean diameter, d_{32}, and impeller Weber number can be correlated with the exponent of –0.6. Unlike this, Rodgers and Cooke (2012) proposed the shear tip speed as a correlating parameter for d_{32} diameter dependence on mixing intensity. However, the parameters characterizing DSD are usually determined in equilibrium state only and the effect of the position of droplet measurement is not taken into account. Moreover, the experimental data can not be interpreted in some cases using these models as reported by Bałdyga and Podgórska (1998). According to Bałdyga and Bourne (1993; 1995), the fine-scale properties of turbulence are responsible for these effects. Bałdyga and Podgórska (1998) proposed a model predicting drop size breaking in the inertial subrange of turbulent and taking internal intermittency into account.

We tested the liquid–liquid dispersion homogeneity in a vessel agitated by a high-shear sawtooth impeller in our previous work (Formánek and Šulc, 2019c; 2020). Three regions of interest placed in the different off-bottom distances were chosen, where the droplet sizes were measured. The time evolution of Sauter mean diameter and DSD evolution were evaluated for homogeneity analysis. It was found that the measured droplet sizes depend on the location of the investigated area. Following on from that, the investigated area or sampling point should be located concerning the flow in the agitated vessel. We similarly tested the dispersion homogeneity in a vessel agitated by a Rushton turbine at 200 rpm impeller speed in our previous work (Formánek et al., 2019a). We found that the droplets observed in the third region placed at the top of the vessel were different compared with regions located near the turbine where the droplets and DSD were practically the same.

We, therefore, analyzed dispersion homogeneity formed by a Rushton turbine in more detail. The results for three impeller speeds, 250, 300, and 350 rpm, are presented here. The time evolution of Sauter mean diameter, d_{32}, and DSD were investigated in three different regions. For Sauter mean kinetics, the model proposed by Hong and Lee (1983) was used. Using this model, the equilibrium Sauter mean diameter, d_{32eq}, was estimated. Finally, the dependence of the evaluated equilibrium Sauter mean diameter on the impeller Weber number was compared with i) the correlation proposed by Chen and Middleman (1967) based on Hinze–Kolmogorov theory, and ii) the correlation proposed by Bałdyga and Podgórska (1998) based on internal intermittency for which multifractal exponent α_{FT} was evaluated using measured experimental data.

2. EXPERIMENTAL

The experiments were performed in a fully baffled cylindrical vessel of 300 mm in inner diameter with a flat bottom. The experimental device arrangement is shown in Figure 1. An immiscible liquid system of distilled water and silicone oil (Wacker AP200) was agitated by a Rushton turbine with a diameter of 100 mm. The liquid level height was equal to the inner vessel diameter. The vessel was located in the middle of the square optical box that eliminated image distortion. Dimensions and placement of the regions of interest are shown in Figure 2.

The non-intrusive optical method was used for in-situ measurement of drop size. The method is based on capturing images during the dispersion with a high-speed camera and subsequent evaluation of the captured images via Image Analysis (IA). The experimental procedure was performed in these steps:

- setting of experimental apparatus and capturing device,
- capturing the scale for the image resolution evaluation,
- calibration of IA settings via recording the mixed nylon spheres with precise diameter d_s = 1.19 mm (Figure 3b),

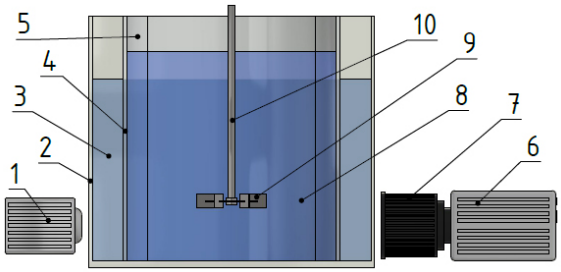

Fig. 1. Arrangement of experimental device: 1 – Single-point light source, 2 – Square optical vessel (glass), 3 – Distilled water, 4 – Cylindrical vessel (glass), 5 – Baffles, 6 – High-speed camera (SpeedSence MKIII – Dantec Dynamics, Denmark), 7 – Objective (Sigma 105 mm F2.8 EX DG MACRO), 8 – Distilled water – Silicone oil (WACKER AP200), 9 – Rushton Turbine, 10 – Shaft powered by speed control unit IKA EUROSTAR POWER

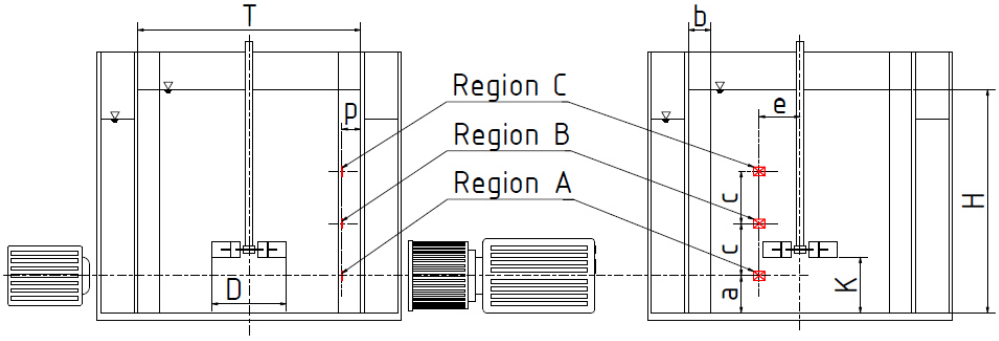

Fig. 2. Scheme of region placement and device dimensions: vessel inner diameter $T = 300$ mm, impeller diameter $D = T/3$, baffle width $b = 0.1T$, liquid level $H = T$, impeller off-bottom distance $K = T/4$, region A off-bottom distance $a = 50$ mm, distance between regions $c = 70$ mm, distance of regions from vessel wall $p = 25$ mm, region distance from the shaft $e = 55$ mm

- recording of image sets during the dispersion, and
- evaluation of drop size via IA. The image resolution was obtained using a 1×1 mm grid placed in each region of interest (Figure 3a).

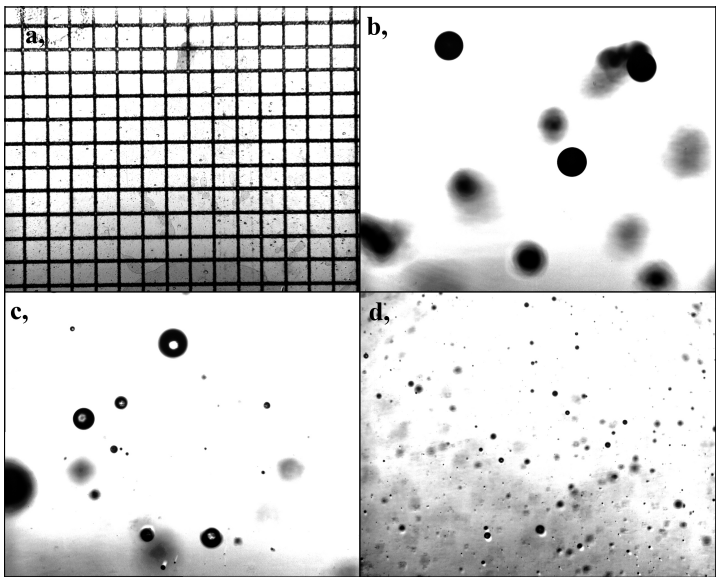

Fig. 3. Calibration procedure and Image Analysis: a) image with captured 1×1 mm grid for image resolution evaluation, b) image with captured Nylon spheres for calibration of image analysis settings, c) raw image captured at recording time of 5 min at 250 rpm impeller speed in Region C, d) raw image captured at recording time of 40 min at 350 rpm impeller speed in Region C

During the dispersion process, the batch temperature rises due to energy dissipation of the propeller and light source. The temperature growth of 0.5 °C was observed during the process thanks to the usage of the LED light source (Formánek et al., 2019b). The mean temperature was 21 °C. The values of needed physical properties for both continuous and dispersed phases are presented in Table 1.

Table 1. Physical properties of the immiscible liquid–liquid system

Phase	Density ρ [kg m^{-3}]	Viscosity μ [mPa s]	Surface tension σ [mN m^{-1}]	Volume fraction φ [–]
Continuous	998	0.98	72.14	0.99953
Dispersed	1076.75	232	26.43	0.00047

A high-speed camera captured images of resolution 1280 × 1024 pixels at a rate of 30 frames per second (fps) with a shutter speed of 3 µs.

The effect of the cylindrical vessel wall on image distortion was eliminated with an optical box. Both the camera and the objective had no effect on image distortion in their combination. The focus depth of the camera-objective configuration of 1.75 mm was determined experimentally. The difference between captured sphere with 1 mm in diameter on the front and back area of the captured region was less than 0.3% which had minimal influence on image analysis, and thus could be neglected.

Three regions of interest were chosen for the investigation of dispersion homogeneity level during the emulsification (Figure 2). The parameters of investigated areas are presented in Table 2. For each region (Region A, B, and C) and each impeller rotation, 8 image sets (1 set = 1000 images) were captured repeatedly after 5 min, thus the total time of measurement was 40 minutes for each region, and each impeller rotation speed. When the 8 image sets were captured, the impeller speed was increased by a jump. In this way, the following sequence of image sets was captured in each region: 1 to 8 image sets for 250 rpm (Re = 42432), 9 to 16 image sets for 300 rpm (Re = 50918), and 17 to 24 image sets for 350 rpm (Re = 59405).

Table 2. Parameters of investigated regions

Region	Area [mm × mm]	Image Resolution [mm pixel^{-1}]	NoED[1] [–]
A	15.043 × 12.034	0.011752	1 090 983
B	15.094 × 12.075	0.011792	687 316
C	15.063 × 12.051	0.011768	722 026

[1] Total number of evaluated drops in all sets in each region

The impeller speed range was limited on the one hand by the sedimentation of the continuous phase, and on the other side by aeration of a mixed system and mechanical stiffness of the experimental apparatus.

The evaluation of drop size from captured images via Image Analysis is the last step of the measurement procedure.

The evaluating method used is based on the comparison of pixel shade gradients between adjacent pixels. The gradients between sharp drop edge and background are significantly higher than the drop out of focus

and background which guarantees the evaluation only focused on drop inside the focus depth. The droplets captured outside the focal depth can be responsible for incorrect DSD determination. The second important parameter of the evaluation was circularity. The circularity was set on the value of 0.95 which means that the objects with circularity less than 0.95 were excluded from the counting.

For illustration, the raw images at recording time of 40 min at the impeller rotations of 250 and 350 rpm in Region C are shown in Figures 3c and 3d. Finally, the area of identified drops was evaluated. More details about the method of measurement and experimental apparatus are given in our previous papers (Formánek et al., 2019a; 2019b).

3. RESULTS AND DISCUSSION

3.1. Number of evaluated drops

Bucciarelli et al. (2019) found a minimum number of drops that exist that must be reached to obtain relevant results. The total number of evaluated drops given in Table 2 represents the sum of identified drops from 24 000 captured images (8 sets of 1000 images for each impeller speed). The time courses of the number of evaluated drops are shown in Figure 4 for 250, 300, and 350 rpm impeller rotation speeds and each region. The number of captured drops grew constantly in each region.

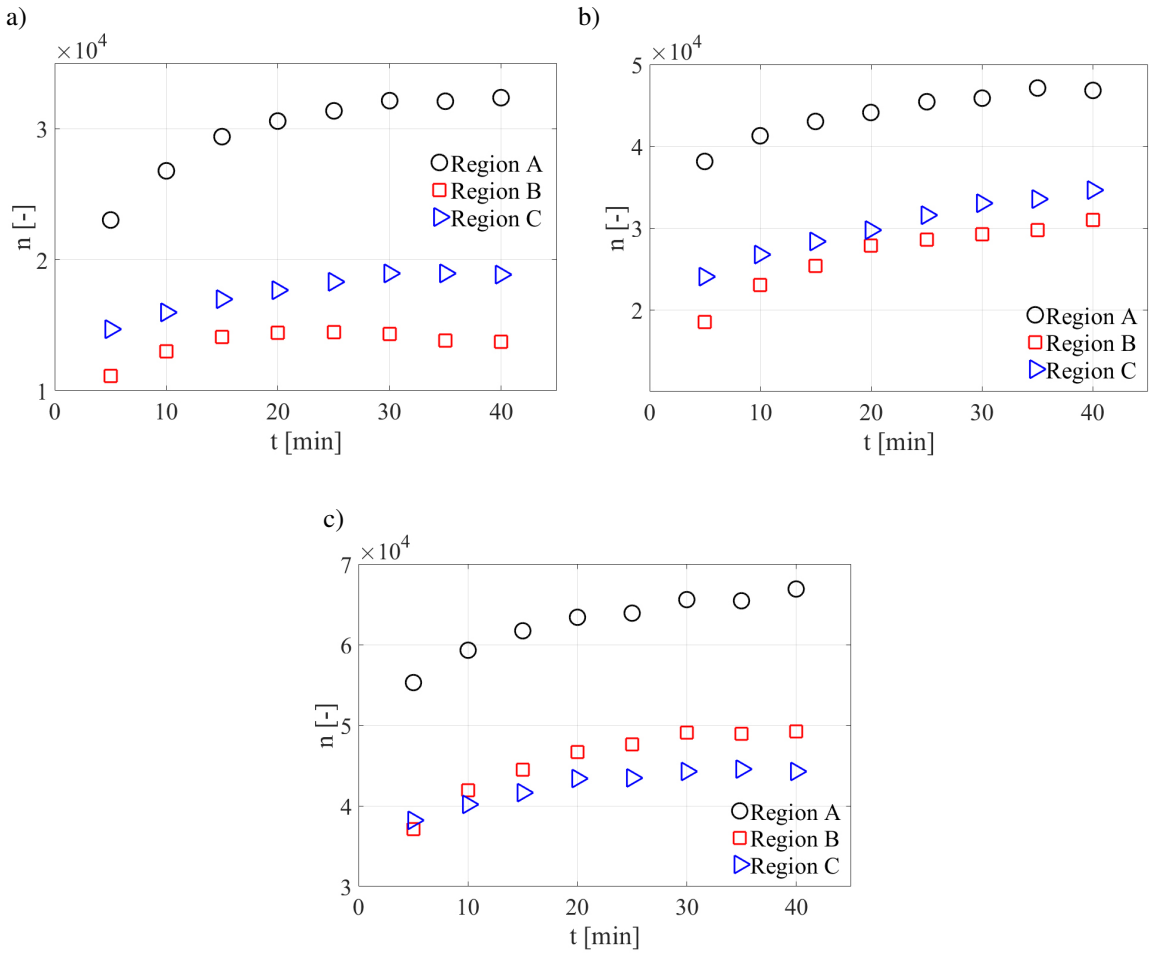

Fig. 4. Time course of the number of evaluated drops: a) 250 rpm impeller rotation speed, b) 300 rpm impeller rotation speed, c) 350 rpm impeller rotation speed

The significantly higher number of evaluated drops in Region A compared with Region B was probably caused by different hydrodynamic conditions between regions placed above and below the impeller outflowing stream.

3.2. Kinetics of Sauter mean diameter d_{32}

The time evolution of Sauter mean diameter d_{32} is shown in Figure 5 for 250, 300, and 350 rpm impeller rotation speeds and each region. For all impeller rotation speeds, the highest values of d_{32} were observed in Region C. The time evolution of d_{32} for 250 rpm impeller speed was practically the same in Regions A and B which were placed at the same distance below and above the impeller. For 300 rpm impeller rotational speed, the differences between the d_{32} values were around 5 μm only in all regions among investigated time steps. For 350 rpm impeller rotational speed, the higher differences between d_{32} values were observed, approx. 10 μm, in all regions among investigated time steps.

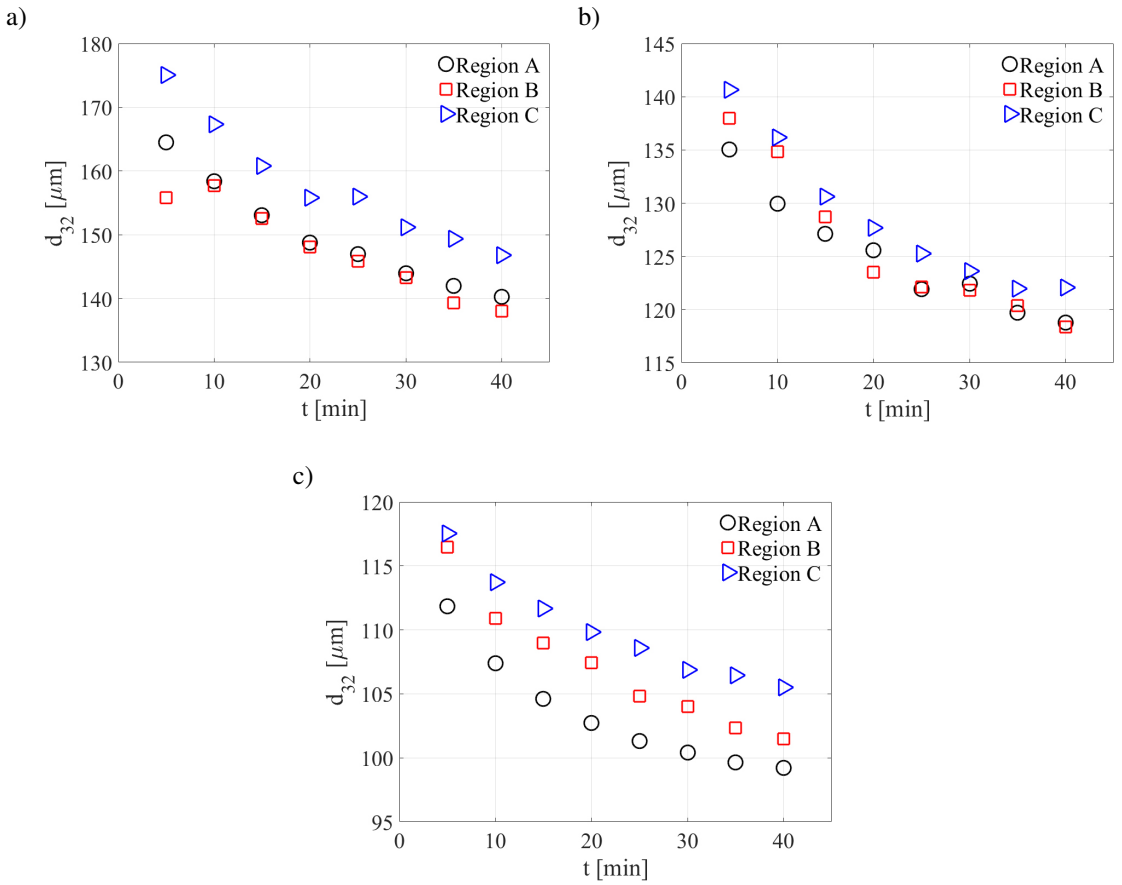

Fig. 5. Time evolution of Sauter mean diameter: a) 250 rpm impeller rotational speed, b) 300 rpm impeller rotational speed, c) 350 rpm impeller rotation speed

For 250 and 300 rpm impeller speeds, the d_{32} values obtained in regions A and B were comparable, as was expected. Unlike this, the different d_{32} values obtained in regions A and B were observed for 350 rpm impeller speed.

Time evolution of d_{32} values was described with the kinetic model proposed by Hong and Lee (1983):

$$\frac{d_{32}}{d_{32\mathrm{eq}}} = 1 + \alpha \cdot \exp\left(-\beta \cdot t^*\right) \tag{1}$$

where $d_{32\mathrm{eq}}$ is the Sauter mean diameter in an equilibrium state, α and β are the model parameters, and t^* is dimensionless dispersion time defined as a product of impeller speed N and dispersion time t.

The model parameters evaluated for experimental data are listed in Table 3 for all regions and impeller rotation speeds.

Table 3. Evaluated parameters of Hong and Lee (1983) kinetic model

Impeller rotational speed (rpm)	Region	d_{32eq} [μm]	α	$\beta \cdot 10^{-4}$
250	A	134.92	0.279	1.917
	B	138.83	0.196	2.316
	C	142.66	0.294	2.129
300	A	115.54	0.211	1.614
	B	115.85	0.267	1.988
	C	118.87	0.253	2.033
350	A	98.31	0.199	2.161
	B	99.08	0.221	1.506
	C	103.48	0.175	1.520

The comparison of experimental and calculated data predicted by Hong and Lee (1983) kinetics model is shown in Figure 6 for 250, 300, and 350 rpm impeller rotation speeds and each region.

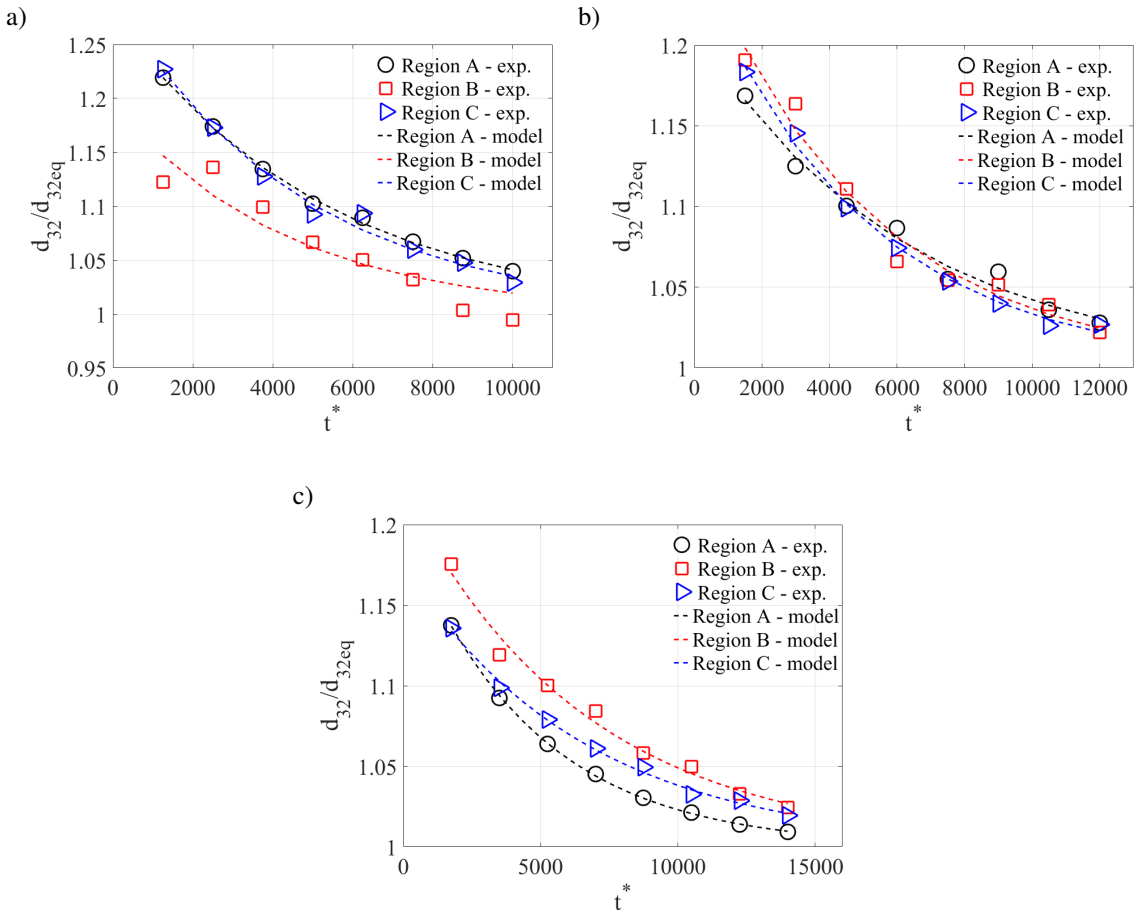

Fig. 6. Comparison of Hong and Lee (1983) kinetics model with experimental data: a) 250 rpm impeller rotational speed, b) 300 rpm impeller rotational speed, c) 350 rpm impeller rotation speed

The following relation between the equilibrium Sauter mean diameter (d_{32eq}) related to the impeller diameter (D) and impeller Weber number (We) can be derived based on the Hinze -Kolmogorov theory of drop-breaking occurring in the inertial subrange:

$$\frac{d_{32eq}}{D} = C_1 \cdot We^{-0.6} \tag{2}$$

where C_1 is the constant of proportionality.

Based on the experimental data, the value of the proportionality constant of 0.07 was evaluated. The comparison of the correlation (2) and calculated d_{32eq} values is shown in Figure 7. For illustration, the correlation reported by Chen and Middleman (1967) is also shown. Chen and Middleman (1967) realized an extensive program of drop size investigation in a vessel stirred by a Rushton turbine for various immiscible liquid–liquid systems and various ratios of D/T. The experiments were carried out in six baffled and flat bottomed cylindrical vessels of the diameter of 4, 6, 8, 10, 12, and 18 inches and agitated by five six-blade Rushton turbines with diameters of 2, 3, 4, 5, and 6 inches. The size of captured drop was measured with a Leeds and Northup galvanometer 2430C in the output impeller stream. Based on these data, they reported the value of proportionality constant $C_1 = 0.053$.

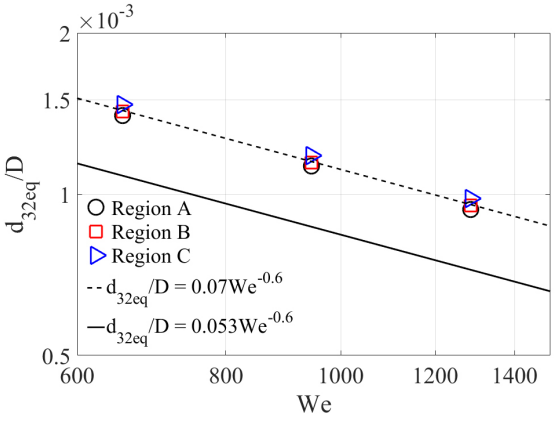

Fig. 7. Dependence of the ratio of d_{32eq}/D on the impeller Weber number

The experiments were carried out sequentially with the jump change of impeller rotational speed. Combining Eqs. (1) and (2), we derived the following relation between model parameter α and jump change of impeller speed from N_1 speed to N_2 speed in the following way:

- assuming that the initial drop size $d_{32}(t = 0)$ for consecutive N_2 impeller speed is equal to the equilibrium size d_{32eq} obtained for previous N_1 impeller speed expressed by Eq. (2),
- the model parameter α can be expressed from Eq. (1) for initial time ($t = 0$) as follows:

$$\alpha = \frac{d_{32eq}(t = 0,\ N_2) - d_{32eq}(N_1)}{d_{32eq}(N_1)} \tag{3}$$

- assuming that the other physical and geometrical parameters are unchanged, thus the following final relation can be obtained

$$\alpha + 1 = \left(\frac{N_2}{N_1}\right)^{1.2} \tag{4}$$

where N_1 is the previous impeller rotational speed, N_2 is the consecutive impeller rotational speed after the speed jump change. The ratio N_2/N_1 for 250 rpm was determined using the previous impeller speed of 200 rpm. The comparison of experimental values and this prediction is shown in Figure 8.

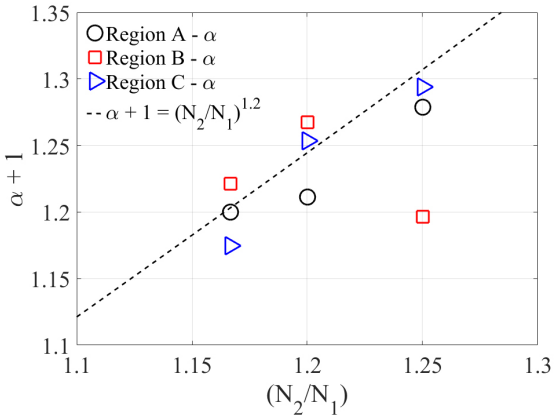

Fig. 8. Dependence of kinetics model parameter α as a function of impeller speed ratio N_2/N_1

The kinetics model parameter β was empirically fitted by a power-law function as a function of impeller Weber number:

$$\frac{\beta}{N} = C_2 \cdot \mathrm{We}^{-0.6} \tag{5}$$

where the constant of proportionality $C_2 = -3.937 \cdot 10^{-5}$ was evaluated. The comparison of the proposed correlation and evaluated kinetics model parameter β is shown in Figure 9.

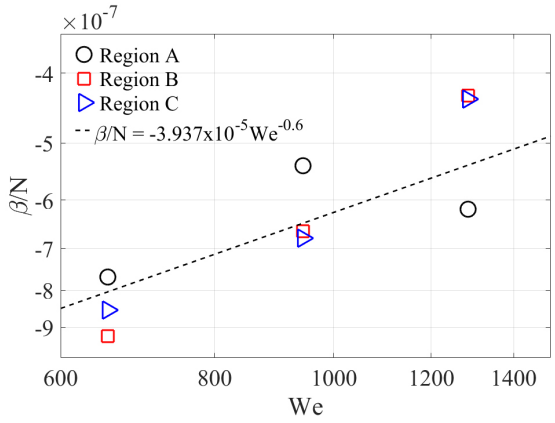

Fig. 9. Dependence of kinetics model parameter β as a function of impeller Weber number

3.3. Frequency drop size distribution time evolution

The frequency drop size distribution was chosen as a second criterion for the dispersion homogeneity assessment. The frequency DSDs were evaluated and presented in Figure 10 as functions of the logarithm scale of drop size for investigated impeller rotation speeds and each region. For better readability, the distribution curves were rendered only in initial and ending measuring time steps, e.g. in the beginning at the time step $t = 5$ min. and at the end at $t = 40$ min. for all regions of interest.

The distribution curves practically do not change up to approximately 100 µm drop size for the tested rotation impeller speeds regardless of the investigated region. The curves differ only in the absolute value of size-frequency for each impeller speed. It indicates that no drop size changes practically occur for the smallest drop classes. The changes of drop sizes occurring during dispersion are visible only for higher drop sizes greater than approx. 160–200 µm. In this case, the difference among investigated regions was observed. In the middle size range approx. from 100 to 200 µm, the transient changes occured.

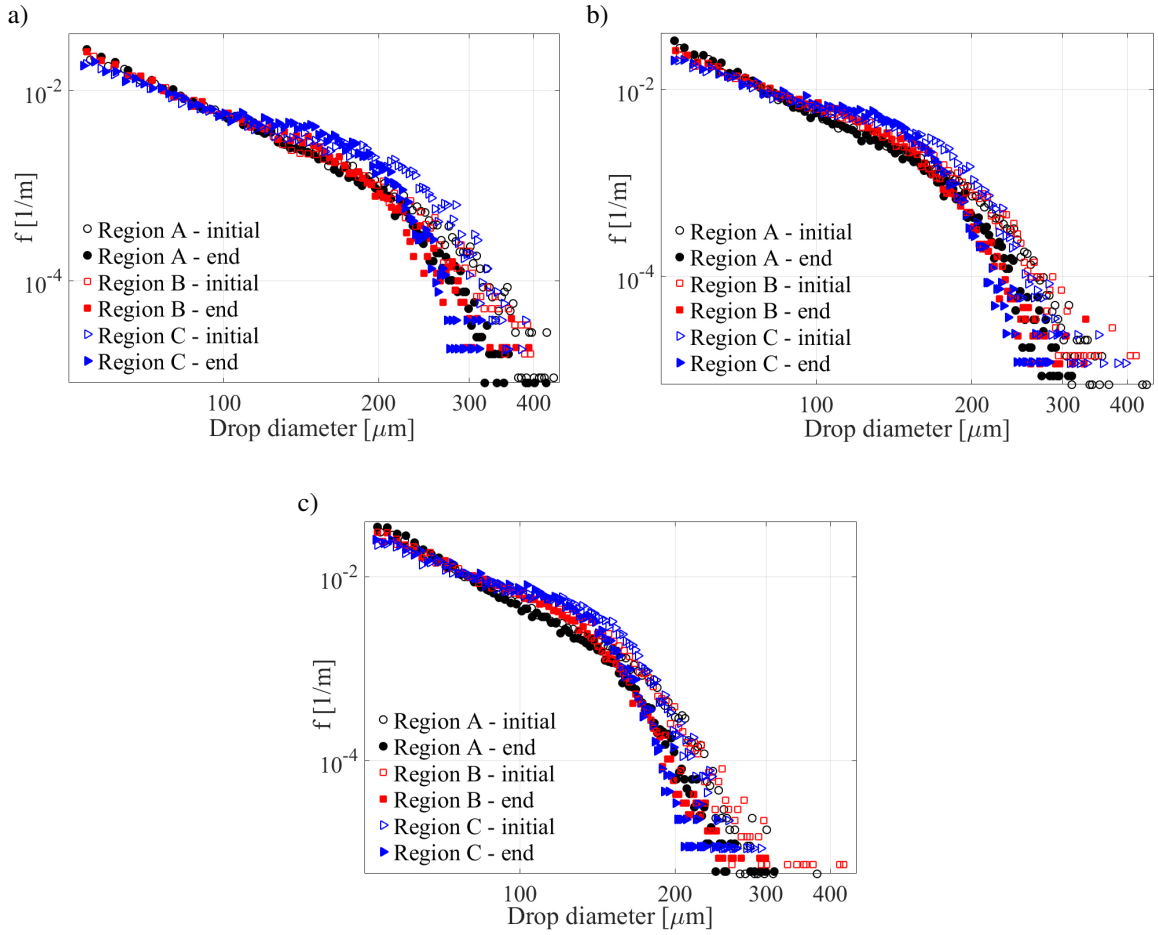

Fig. 10. Frequency drop size distribution evolution at the beginning and at the end of a measured time step for three regions of interest: a) 250 rpm impeller rotational speed, b) 300 rpm impeller rotational speed, c) 350 rpm impeller rotation speed

3.4. Effect of internal intermittency

For a vessel agitated by a Rushton turbine, the fully turbulent regime can be expected for a Reynolds number greater than 50,000 (Šulc et al., 2015; 2017). The experiments were carried out in the range of Reynolds numbers from 42432 to 59405. Therefore, the anisotropic turbulent flow may exist in the vessel, especially in the impeller zone. Therefore, we speculatively tested the effect of internal intermittency on dispersion performance.

Bałdyga and Podgórska (1998) proposed the following relation between maximum stable drop size $d_{\max}$ in dilute non-coalescing liquid–liquid dispersion for drop breaking occurring in the inertial subrange of turbulent and taking internal intermittency into account:

$$\frac{d_{\max}}{D} = C_3 \cdot \mathrm{We}^{\frac{-0.6}{1-0.4\cdot(1-\alpha_{FT})}} \tag{6}$$

where α_{FT} is the multifractal exponent.

For the value of multifractal exponent $\alpha_{FT} = 1$, the exponent of Weber number in Equation (6) is equal to –0.6 and corresponds to Hinze–Kolmogorov theory assuming local isotropy state.

The value of α_{FT} lower than 1 indicates that the vorticity and turbulent stresses are not distributed uniformly (this phenomenon is named “internal intermittency” or “fine-scale intermittency”).

The question arises, how to determine maximum drop size, $d_{\max}$. We evaluated maximum drop size from the relative cumulative frequency distribution curves obtained at the end of a measured time step, by definition, for the cumulative percentage of 95%, 97%, 99%, 99.3%, 99.5%, 99.7%, and 99.9% 4 for each region and impeller rotational speed. For comparison, the maximum drop size was also estimated as an average of 1% of the number of largest drops (denoted as $d_{99\text{avg}}$). The maximum drop sizes estimated by this procedure were correlated with the impeller Weber number using Eq. (6). The calculated multifractal exponents α_{FT} are presented in Table 4 for each region and graphically in Figure 11. It was found that the method used for $d_{\max}$ estimation significantly affected the α_{FT} estimation. Following on from that, the correct determination of maximum drop size is a crucial factor for the correct estimation of multifractal exponent α_{FT}. We decided, therefore, to determine multifractal exponent α_{FT} by extrapolation of partial values to cumulative 100%. The extrapolated α_{FT} values are presented in Table 4.

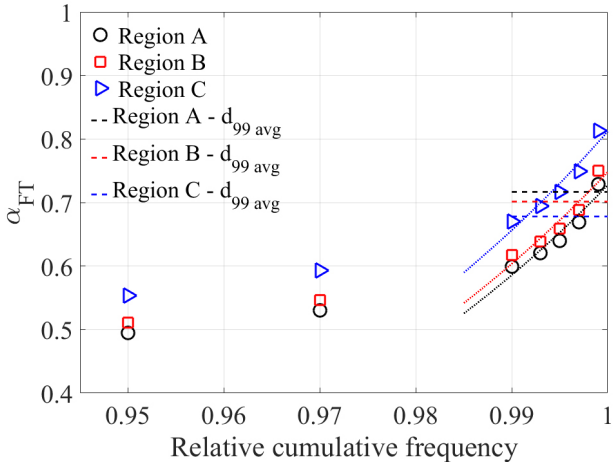

Fig. 11. The dependency of multifractal exponent α_{FT} on the determined value of $d_{\max}$ from relative cumulative frequency

Table 4. Estimation of multifractal exponent α_{FT}

Region		d_{95}	d_{97}	d_{99}	$d_{99.3}$	$d_{99.5}$	$d_{99.7}$	$d_{99.9}$	$d_{99\text{avg}}$ [1]	$d_{100\text{extr}}$ [2]
A	α_{FT}	0.49	0.53	0.60	0.62	0.64	0.67	0.73	0.72	0.73
B	α_{FT}	0.51	0.55	0.62	0.64	0.66	0.69	0.75	0.7	0.75
C	α_{FT}	0.55	0.59	0.67	0.69	0.72	0.75	0.81	0.67	0.81

[1] Average of 1% of the number of largest drops

[2] Extrapolated value of α_{FT} for 100% cumulative value

The higher values of multifractal exponent α_{FT} were evaluated in Region C. The α_{FT} values estimated in regions A and B are practically the same. Compared with region C, the α_{FT} values in regions A and B are approximately by 14% and 10% smaller, respectively.

The lower α_{FT} values estimated in regions A and B indicate more vigorous flow and drop breaking in the impeller zone, as expected.

Finally, α_{FT} values far from 1 indicate that stresses acting on the drop break-up are higher, and maximum stable drop size may not be achieved.

4. CONCLUSIONS

The homogeneity of the diluted immiscible liquid–liquid system was investigated in a fully baffled and flat-bottomed cylindrical vessel agitated by a Rushton turbine. The mixture of the distilled water and silicone oil was used as a model system. The non-intrusive optical method utilizing image analysis was used for drop size determination.

As criteria of dispersion homogeneity in the liquid–liquid system, the scales of parity were used between evaluated Sauter mean diameters, drop size distribution, and multifractal exponent in three regions differently placed in the vessel.

For the tested impeller rotation speeds, higher d_{32} values were observed in Region C compared to regions A and B placed in the impeller outgoing stream.

The dependence of $d_{32\mathrm{eq}}/D$ ratio on the impeller Weber number was correlated using $\mathrm{We}^{-0.6}$ relation derived from the Hinze–Kolmogorov theory. Based on the experimental data, the value of the proportionality constant of 0.07 was evaluated. This value is 1.33 times higher compared with Chen and Middleman (1967).

The time evolution of frequency drop size distribution was used as a second criterion of homogeneity investigation. The distribution curves practically did not change up to approximately 100 μm drop size for tested rotation impeller speeds regardless of investigated region. The changes of drop sizes occurring during dispersion are visible only for higher drop sizes. In this case, the difference among investigated regions was observed.

Finally, the effect of intermittency turbulence on drop size reported by Bałdyga and Podgórska (1998) was analyzed and the multifractal exponent α_{FT} was evaluated. The α_{FT} value of approx. 0.73 was found for regions A and B. Unlike this, the higher α_{FT} value (0.81) was estimated for region C. The lower α_{FT} value estimated in regions A and B indicates more vigorous flow and drop breaking in the impeller zone, as expected.

The results obtained confirm that measured droplet sizes depend on the location of the investigated area. The investigated area or sampling point should be located concerning the flow in the agitated vessel. Similar results were found for a high-shear sawtooth impeller in our previous research.

SYMBOLS

a	distance of the region A from the vessel bottom, m
b	baffle width, m
c	distance between regions, m
C	constant of proportionality, –
D	impeller diameter, m,
d	drop diameter, m
d_{32}	Sauter mean diameter, m
$d_{32\mathrm{eq}}$	equilibrium Sauter mean diameter, m
$d_{\max}$	maximum stable drop size, m
d_s	calibration sphere diameter, m
e	region distance from the vessel axis, m
H	liquid level, m
K	impeller clearance, m

N	impeller speed, 1/s
n	number of evaluated drops, –
p	region distance from the vessel wall, m
Re	impeller Reynolds number (Re = $\rho_c N D^2/\mu_c$), –
t	time of measurement, s
t^*	dimensionless dispersion time ($t^* = Nt$), –
T	vessel diameter, m
We	impeller Weber number (We = $\rho_c N^2 D^3/\sigma$), –

Greek symbols

α	model parameter, –
α_{FT}	multifractal exponent, –
β	model parameter, –
μ	dynamic viscosity, Pa s
ρ	density, kg/m^3
σ	surface tension, N/m^1
φ	volume fraction, –

Subscripts

1, 2, 3	number of components
95, 97, 99, 99.3, 99.5, 99.7, 99.9, 100	relative cumulative frequency value
c	continuous phase
d	dispersed phase
extr	extrapolated value

ACKNOWLEDGMENTS

This work was supported by GA CTU SGS project number SGS20/119/OHK2/2T/12 "Transport phenomena in multiphase systems" and by the Ministry of Education, Youth and Sports of the Czech Republic under OP RDE grant number CZ.02.1.01/0.0/0.0/16_019/0000753 "Research center for low-carbon energy technologies".

REFERENCES

Bałdyga J., Bourne J.R., 1993. Drop breakup and intermittent turbulence. *J. Chem. Eng. Japan*, 26, 738–741. DOI: 10.1252/jcej.26.738.

Bałdyga J., Bourne J.R., 1995. Interpretation of turbulent mixing using fractals and multifractals. *Chem. Eng. Sci.*, 50, 381–400. DOI: 10.1016/0009-2509(94)00217-F.

Bałdyga J., Podgórska W., 1998. Drop break-up in intermittent turbulence. Maximum stable drop size and transient sizes of drops. *Can. J. Chem. Eng.*, 76, 456–470. DOI: 10.1002/cjce.5450760316.

Bucciarelli E., Formánek R., Kysela B., Fořt I., Šulc R., 2019. Dispersion kinetics in mechanically agitated vessel. *EPJ Web Conf.*, 213, 02008. DOI: 10.1051/epjconf/201921302008.

Chen H.T., Middleman S., 1967. Drop size distribution in agitated liquid–liquid systems. *AIChE J.*, 13, 989–995. DOI: 10.1002/aic.690130529.

Formánek R., Kysela B., Šulc R., 2019a. Drop size evolution kinetics in a liquid–liquid dispersions system in a vessel agitated by a Rushton turbine. *Chem. Eng. Trans.*, 74, 1039–1044. DOI: 10.3303/CET1974174.

Formánek R., Kysela B., Šulc R., 2019b. Image analysis of particle size: effect of light source type. *EPJ Web Conf.*, 213, 02021. DOI: 10.1051/epjconf/201921302021.

Formánek R., Šulc R., 2019c. Dispersion of immiscible liquid–liquid system in a vessel agitated by a Sawtooth impeller: Drop size time evolution. *Proceedings of the International Conference Experimental Fluid Mechanics 2019*. Franzensbad, Czech Republic, 19–22 November 2019, 136–139.

Formánek R., Šulc R., 2020. The liquid–liquid dispersion homogeneity in a vessel agitated by a high-shear sawtooth impeller. *Processes*, 8, 1012. DOI: 10.3390/pr8091012.

Hinze J.O., 1955. Fundamentals of the hydrodynamic mechanism of splitting in dispersion processes. *AIChE J.*, 1, 289–295. DOI: 10.1002/aic.690010303.

Hong P.O., Lee J.M., 1983. Unsteady-state liquid–liquid dispersions in agitated vessels. *Ind. Eng. Chem. Process Des. Dev.*, 22, 130–135. DOI: 10.1021/i200020a021.

Jasikova D., Kotek M., Kysela B., Sulc R., Kopecky V., 2018. Compiled visualization with IPI method for analysing of liquid–liquid mixing process. *EPJ Web Conf.*, 180, 02039. DOI: 10.1051/epjconf/201818002039.

Khalil A., Puel F., Chevalier Y., Galvan J.-M., Rivoire A., Klein J.-P., 2010. Study of droplet size distribution during an emulsification process using in situ video probe coupled with an automatic image analysis. *Chem. Eng. J.*, 165, 946–957. DOI: 10.1016/j.cej.2010.10.031.

Kolmogorov A.N., 1949. On the breakage of drops in a turbulent flow. *Dokl. Akad. Nauk SSSR*, 66, 825–828.

Kraume M., Gäbler A., Schulze K., 2004. Influence of physical properties on drop size distribution of stirred liquid–liquid dispersions. *Chem. Eng. Technol.*, 27, 330–334. DOI: 10.1002/ceat.200402006.

Maaß S., Kraume M., 2012. Determination of breakage rates using single drop experiments. *Chem. Eng. Sci.*, 70, 146–164. DOI: 10.1016/j.ces.2011.08.027.

Malík M., Primas J., Kotek M., Jašíková D., Kopecký V., 2019. Mixing of two immiscible phases measured by industrial electrical impedance tomography system. *Mech. Ind.*, 20, 707. DOI: 10.1051/meca/2019081.

Maluta F., Montante G., Paglianti A., 2020. Analysis of immiscible liquid–liquid mixing in stirred tanks by Electrical Resistance Tomography. *Chem. Eng. Sci.*, 227, 115898. DOI: 10.1016/j.ces.2020.115898.

Pacek A.W., Chamsart S, Nienow A.W., Bakker A., 1999. The influence of impeller type on mean drop size and drop size distribution in an agitated vessel. *Chem. Eng. Sci.*, 54, 4211–4222. DOI: 10.1016/S0009-2509(99)00156-6.

Rodgers T.L., Cooke M., 2012. Correlation of drop size with sheat tip speed. *14th European Conference on Mixing*. Warszawa, Poland, 10–13 September 2012, 407–412.

Šulc R., Ditl P., Fořt I., Jašíkova D., Kotek M., Kopecký V., Kysela B., 2017. Local velocity scaling in T400 vessel agitated by Rushton turbine in a fully turbulent region. *EPJ Web Conf.*, 143, 02120. DOI: 10.1051/epjconf/201714302120.

Šulc R., Pešava V., Ditl P., 2015. Local turbulent energy dissipation rate in a vessel agitated by a Rushton turbine. *Chem. Process Eng.*, 36, 135–149. DOI: 10.1515/cpe-2015-0011.

Zhou G, Kresta S.M., 1998. Evolution of drop size distribution in liquid–liquid dispersions for various impellers. *Chem. Eng. Sci.*, 53, 2099–2113. DOI: 10.1016/S0009-2509(97)00437-5.

Received 15 June 2021
Received in revised form 11 August 2021
Accepted 24 August 2021